



INTERNATIONAL ATOMIC ENERGY AGENCY
UNITED NATIONS EDUCATIONAL, SCIENTIFIC AND CULTURAL ORGANIZATION
INTERNATIONAL CENTRE FOR THEORETICAL PHYSICS
I.C.T.P., P.O. BOX 586, 34100 TRIESTE, ITALY, CABLE: CENTRATOM TRIESTE



SMR.755/27

Workshop on Fluid Mechanics

(7 - 25 March 1994)

**Spatio-temporal instabilities
in closed and open flows**

P. Huerre
Laboratoire d'Hydrodynamique
Ecole Polytechnique
91128 Palaiseau
France

These are preliminary lecture notes, intended only for distribution to participants



SPATIO-TEMPORAL INSTABILITIES IN CLOSED AND OPEN FLOWS

P. Huerre
Department of Aerospace Engineering
University of Southern California
Los Angeles, California 90089-0192
U.S.A.

ABSTRACT. A review is given of the general theory describing the linear evolution of spatio-temporal instability waves in fluid media. According to the character of the impulse response, one can distinguish between absolutely unstable (closed) flows and convectively unstable (open) flows. These notions are then applied to several evolution models of interest in weakly nonlinear stability theory. It is argued that absolutely unstable flows, convectively unstable flows and mixed flows exhibit a very different sensitivity to external perturbations. Implications of these concepts to frequency selection mechanisms in mixed flows and the onset of chaos in convectively unstable flows are also discussed.

1. INTRODUCTION

In hydrodynamics, one often distinguishes between the behavior of closed systems and open systems without being too specific about the meaning of these concepts. From a purely kinematic point of view, one is tempted to say that a flow is closed when fluid particles are recycled within the physical domain of interest. If all fluid particles ultimately leave the domain, the flow is said to be open. On such grounds, Bénard convection within a horizontal fluid layer is a closed system whereas plane Poiseuille flow, wakes, jets, etc... are open systems.

In the present review, closed and open flows will be defined instead with respect to the character of the hydrodynamic instabilities which they can support. Thus, the motion of waves is claimed to be more relevant than the motion of fluid *particles*. Following Briggs [1] and Bers [2], a flow will be said to be absolutely unstable (closed) if its impulse response is unbounded everywhere for large time (Figure 2b). If the impulse response decays to zero at all spatial locations, the flow will be said to be convectively unstable (open) (Figure 2c). These notions will be defined and reviewed in detail in section 2. In other words, from a hydrodynamic stability point of view, closed and open systems refer to absolutely unstable and

convectively unstable flows, respectively. In the core of this paper, we shall use this latter terminology only.

It should be made clear that a given flow can be open with respect to fluid particle trajectories but closed (absolutely unstable) with respect to instability waves. For instance, a parallel wake flow with a sech^2 velocity profile is absolutely unstable for large values of the velocity deficit [3], see discussion of section 4.3. Yet, fluid particles clearly move out of the physical domain and no recycling of particles takes place. Similarly, parallel axisymmetric hot jets are absolutely unstable if the core temperature is sufficiently higher than the ambient temperature [4,5]. Here again, fluid particles move downstream but hydrodynamic instability waves contaminate the entire medium. Thus, in many cases, one must rely on *mathematical* criteria to determine whether a given flow is absolutely unstable or convectively unstable. These criteria which were first proposed by Briggs [1] in the context of plasma instabilities are discussed in section 2.

In section 3, the general method is illustrated on three amplitude evolution models commonly arising in the context of hydrodynamic instabilities: the Ginzburg-Landau equation, the Klein-Gordon equation and the long-wavelength integro-differential equation obtained in reference [6]. The implications of these notions to receptivity issues, frequency selection mechanisms and chaos in open flows are critically reviewed in section 4.

For a recent review of similar topics within the context of shear flows, the reader is referred to [7].

2. GENERAL FORMALISM

The main concepts will first be developed in the general context of spatio-temporal waves in one-dimensional space. The development broadly follows the review of Bers [2]. Let $A(x,t)$ be a scalar function of space coordinate x and time t , which may represent for instance the fluctuating velocity or temperature field in a fluid medium. More generally, $A(x,t)$ could be a column vector with an arbitrary number of components. For simplicity, $A(x,t)$ is assumed here to have a single component only and to satisfy a differential equation of the form

$$D \left[-i \frac{\partial}{\partial x}, i \frac{\partial}{\partial t}; R \right] A(x,t) = S(x,t), \quad (1)$$

where D is a *linear* differential operator arising from a perturbation analysis around some basic state of the medium. The function $S(x,t)$ specifies the excitation imposed on the system in some region of space for a given length of time. We assume that $S(x,t) = 0$ everywhere when $t < 0$. The flow may depend on an external control parameter R , such as the Reynolds number, Rayleigh number, etc...

Fourier-transform pairs in space x and time t are then introduced, according to the definition

$$A(x,t) = \frac{1}{(2\pi)^2} \int_F \int_L A(k,\omega) e^{i(kx-\omega t)} d\omega dk. \quad (2)$$

In equation (2), the path F in the complex plane of wavenumbers k is initially taken to be the real axis. The contour L in the complex frequency plane is chosen so that causality is satisfied, namely $A(x,t) = 0$ everywhere when $t < 0$: it is a straight line lying above all the singularities of the complex ω plane. When $t < 0$, the L contour can then be closed by a semicircle above L and the response $A(x,t)$ is identically zero. A sketch of the paths of integration is included in Figure 1.

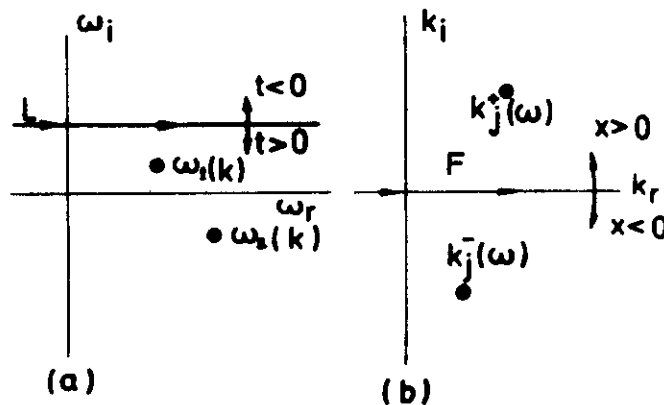


Figure 1. Paths of integration of the inverse Fourier transforms (2): (a) complex frequency plane; (b) complex wavenumber plane.

The Fourier transform of equation (1) readily provides a statement of the problem in the spectral domain:

$$D[k,\omega;R]A(k,\omega) = S(k,\omega). \quad (3)$$

In the absence of forcing, $S(x,t) = S(k,\omega) \equiv 0$, one obtains the *normal modes* of the system in the form of a complex dispersion relation

$$D[k,\omega;R] = 0 \quad (4)$$

between wavenumber k and frequency ω . When k is taken to be real, the zeroes of the dispersion relation yield a collection of *temporal normal modes* with complex eigenvalues $\omega_j(k)$, $j = 1, 2, 3, \dots$. Conversely, when ω is given real, one obtains *spatial branches* $k_j^+(\omega)$, $k_j^-(\omega)$, etc. Both sets play a crucial role in the evaluation of the Green's function as discussed in the next section.

In the forced problem, one can immediately solve for $A(k,\omega)$ in (3) to arrive at a purely formal expression of the solution in terms of the

inverse Fourier transform (2):

$$A(x,t) = \frac{1}{(2\pi)^2} \int_F \int_L \frac{S(k,\omega)}{D(k,\omega;R)} e^{i(kx-\omega t)} d\omega dk, \quad (5)$$

the essential problem being the evaluation of the integrals along L and F!

2.1. Spatio-temporal evolution: The Green's function or Impulse response

Let $G(x,t)$ be the response to a unit impulse $\delta(x)\delta(t)$, i.e. the Green's function of the operator D. We recall that the response of a linear system to an arbitrary forcing input $S(x,t)$ can be determined by convolution of G with S over space and time. From equation (1), the Green's function $G(x,t)$ satisfies

$$D \left[-i \frac{\partial}{\partial x}, i \frac{\partial}{\partial t}; R \right] G(x,t) = \delta(x)\delta(t). \quad (6)$$

Equivalently, one obtains in the spectral domain (see (3)):

$$D[k,\omega;R]G(k,\omega) = 1 \quad (7)$$

At this stage, one may follow one's personal taste to choose the order of the inverse Fourier transforms in (5). We shall first perform the integration in ω -space

$$G(k,t) = \frac{1}{2\pi} \int_L \frac{e^{-i\omega t}}{D(k,\omega;R)} d\omega. \quad (8)$$

When $t < 0$, the contour L is closed from above and no residues contribute to $G(k,t)$ so that $G(k,t) = 0$. When $t > 0$, the contour L is closed by a semi-circle at infinity in the lower half ω -plane bounded by L (see Figure 1a). We shall assume, for simplicity, that the only singularities in the integrand are poles arising from the zeroes of the dispersion relation $D(k,\omega;R)$. Since k is given on the real axis F in the complex k -plane, these poles are located at the temporal (k real, ω complex) eigenmodes $\omega_j(k)$, $j = 1, 2, 3, \dots$. Thus the normal modes of the unforced problem naturally arise in the calculation of G to give the residue contributions

$$G(k,t) = -i \sum_j \frac{e^{-i\omega_j(k)t}}{(\partial D / \partial \omega)[k, \omega_j(k); R]}. \quad (9)$$

Inversion of the Fourier transform with respect to k then leads to the wave packet integrals

$$G(x, t) = -\frac{i}{2\pi} \sum_j \int_{-\infty}^{\infty} \frac{e^{i[kx - \omega_j(k)t]}}{(\partial D / \partial \omega)[k, \omega_j(k); R]} dk \quad (10)$$

Each integral can be evaluated for large time, x/t fixed, by applying the method of steepest descent [8,9]. Details very much depend on the nature of $\omega_j(k)$ (see specific applications in section 3). To pursue the formal development, it is assumed that each branch $\omega_j(k; R)$ gives rise to a single stationary point k_j^* satisfying

$$\frac{d\omega_j}{dk}(k_j^*) = \frac{x}{t}. \quad (11)$$

The surface Σ defined by $\phi(k_r, k_i) = \text{Re}\{i(kx/t - \omega_j)\}$ exhibits in (k_r, k_i, ϕ) space a saddle point at $k_r = k_{rj}^*$, $k_i = k_{ij}^*$. The original contour F can be deformed into a steepest descent path issuing from each saddle point k_j^* , provided no hills of the surface Σ are crossed at infinity. Using standard arguments one obtains

$$G(x, t) \sim - (2\pi)^{-1/2} e^{i\pi/4} \sum_j \frac{e^{i[k_j^* x - \omega_j(k_j^*)t]}}{(\partial D / \partial \omega)[k_j^*, \omega_j(k_j^*)] [(d^2 \omega_j / dk^2)(k_j^*)t]^{1/2}}. \quad (12)$$

The Green's function takes the form of a train of wavepackets in the (x, t) -plane. For a given packet, the flow selects, along each ray $x/t = \text{const.}$, a particular wavenumber k_j^* given by (11). The temporal amplification rate of k_j^* along the ray reduces to $\sigma = \text{Im}\{\omega_j(k_j^*) - k_j^* (d\omega_j / dk)(k_j^*)\}$ and may in general be positive or negative. Different situations are now examined.

2.2. A criterion for convective or absolute instability

Consider, for a moment, a dispersion relation with a single normal mode $\omega(k)$. Definitions and results can readily be extended to systems with multiple modes. According to the character of the impulse response $G(x, t)$, one may first distinguish between stable and unstable flows.

A flow is defined as *stable* if

$$\lim_{t \rightarrow \infty} G(x, t) = 0, \text{ along all rays } x/t = \text{const.} \quad (13)$$

In other words, the temporal growth rate $\omega_i(k) \equiv \text{Im}\omega(k)$ of the normal mode is negative for all real wavenumbers, and the response of the system takes the form of a decaying wavepacket, as sketched in Figure 2a.

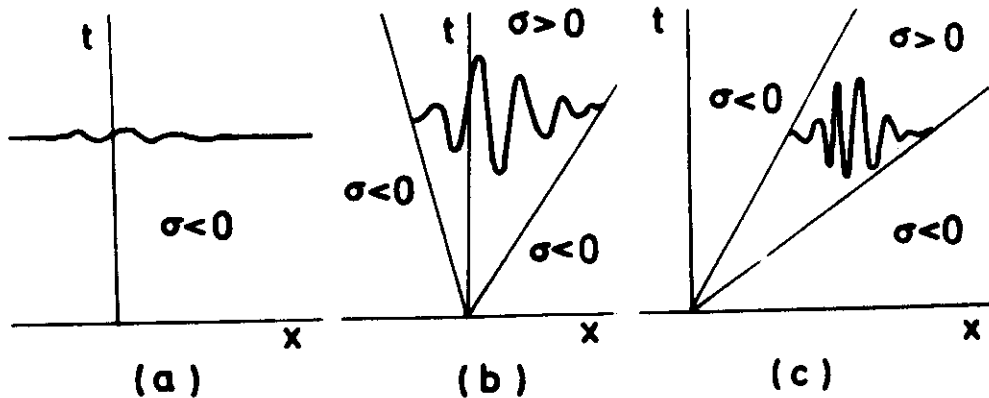


Figure 2. Sketch of impulse responses: (a) stable flow; (b) absolutely unstable flow; (c) convectively unstable flow.

A flow is *unstable* if there exists rays $x/t = \text{const.}$, along which

$$\lim_{t \rightarrow \infty} G(x, t) = \infty. \quad (14)$$

In such a situation, the temporal growth rate $\omega_i(k)$ is positive in some range of real wavenumbers, and the impulse excitation gives rise to an unstable wavepacket confined within a wedge bounded by the two rays of zero amplification rate (see Figures 2b,c). Disturbances grow exponentially in the wedge as given by equation (12). Let k_{max} denote the wavenumber of maximum temporal growth rate such that $(d\omega_i/dk)(k_{\text{max}}) = 0$. As seen from (11), k_{max} travels along the particular ray $x/t = (d\omega_i/dk)(k_{\text{max}})$. The peak of the wavepacket, which grows at the maximum allowable rate $\omega_i(k_{\text{max}})$, therefore moves in that same direction.

But, within the unstable flow category, one must further distinguish between absolute instability and convective instability, as illustrated in Figures 2b and 2c.

An unstable flow is said to be *absolutely unstable* if for all fixed x ,

$$\lim_{t \rightarrow \infty} G(x, t) = \infty. \quad (15)$$

An unstable flow is said to be *convectively unstable* if, for all fixed x ,

$$\lim_{t \rightarrow \infty} G(x, t) = 0. \quad (16)$$

The nature of the instability, is determined by the *long-time* behavior of the wavenumber k_0 staying at a *fixed* spatial location along the ray $x/t = 0$, i.e. the wavenumber of zero group velocity $(d\omega/dk)(k_0) = 0$. Note that, in general, the corresponding complex frequency $\omega_0 = \omega(k_0)$ will be an algebraic branch point of the function $k(\omega)$. In absolutely unstable flows (Figure 2b) the edges of the wavepacket travel in opposite directions and the ray $x/t = 0$ remains in the unstable wedge. Thus, k_0 must have a positive growth rate $\omega_i(k_0) > 0$. Conversely, in convectively unstable flows (Figure 2c) the edges of the packet travel in the same direction, leaving the ray $x/t = 0$ outside the wedge so that $\omega_i(k_0) < 0$. Following Pierrehumbert [10], the quantity $\omega_i(k_0)$ can be called the *absolute growth rate*: $\omega_i(k_0)$ denotes the temporal growth rate of the wavenumber k_0 staying at a fixed x location, whereas $\omega_i(k_{max})$, defined previously, is the temporal growth rate following the peak of the wavepacket. We are led to conclude from the above argument that an unstable flow is convectively unstable when its absolute growth rate is negative: the branch-point singularities of $k(\omega)$ lie in the lower half ω -plane. When the absolute growth rate is positive, the branch points of $k(\omega)$ lie in the upper half ω -plane and the flow is absolutely unstable.

This criterion, however, is not explicit enough as it stands, and one needs to carefully monitor the positions of the zeroes $\omega_j(k)$ and $k_j^{\pm}(\omega)$ of $D(k, \omega)$ located in the ω -plane and k -plane, respectively. To satisfy causality, the contour L in the ω -plane (Figure 1a) can always be placed high enough so that the zeroes $\omega_j(k)$ lie below L when k is real on the initial contour F of Figure 1b. Conversely [2], when ω is on L , none of the zeroes $k_j^+(\omega)$, $k_j^-(\omega)$, etc... of $D(k, \omega)$ in the k -plane can then cross the original contour F . If they did, L itself would intersect one of the curves $\omega_j(k)$ in the ω -plane, which leads to a contradiction. Thus, provided L is high enough, the original F contour neatly separates the spatial branches $k_j^+(\omega)$ and $k_j^-(\omega)$ located in the upper and lower half k -planes. When $x > 0$ ($x < 0$), the contour F is closed in the upper (lower) half k -plane and the residues of the spatial branches $k_j^+(\omega)$ ($k_j^-(\omega)$) contribute. Assume as in the rest of our discussion that a single second-order branch point $\omega_{0,j}$ is associated with each mode $\omega_j(k)$. Two radically distinct situations may then take place.

First, the two Riemann sheets of the branch point $\omega_{0,j}$ may correspond to *spatial branches* $k_j^+(\omega)$ and $k_j^-(\omega)$ located, when L is high enough, on opposite sides of F , i.e., in the upper and lower half k -planes respectively. Then, as L is displaced downward, the curves $k_j^+(\omega)$ and $k_j^-(\omega)$ move towards each other in the k -plane (Figure 3a,b). In this process, one must correspondingly deform the original contour F so as to retain the same number of spatial branches for $x > 0$ and $x < 0$, while at the same time lowering the curve of zeroes $\omega_j(k)$ in the ω -plane. Of course, the simultaneous deformation of L and F must stop when L touches $\omega_j(k)$ and F becomes "pinched" between the branches $k_j^+(\omega)$ and $k_j^-(\omega)$ [2], as sketched in Figure 3c. This is precisely the point $(k_{0,j}, \omega_{0,j})$ identified previously, where the group velocity $d\omega/dk$ is zero. When pinching takes place with $\omega_{0,j}$ still located in the upper ω -plane, the instability is absolute. Otherwise, it is convective.

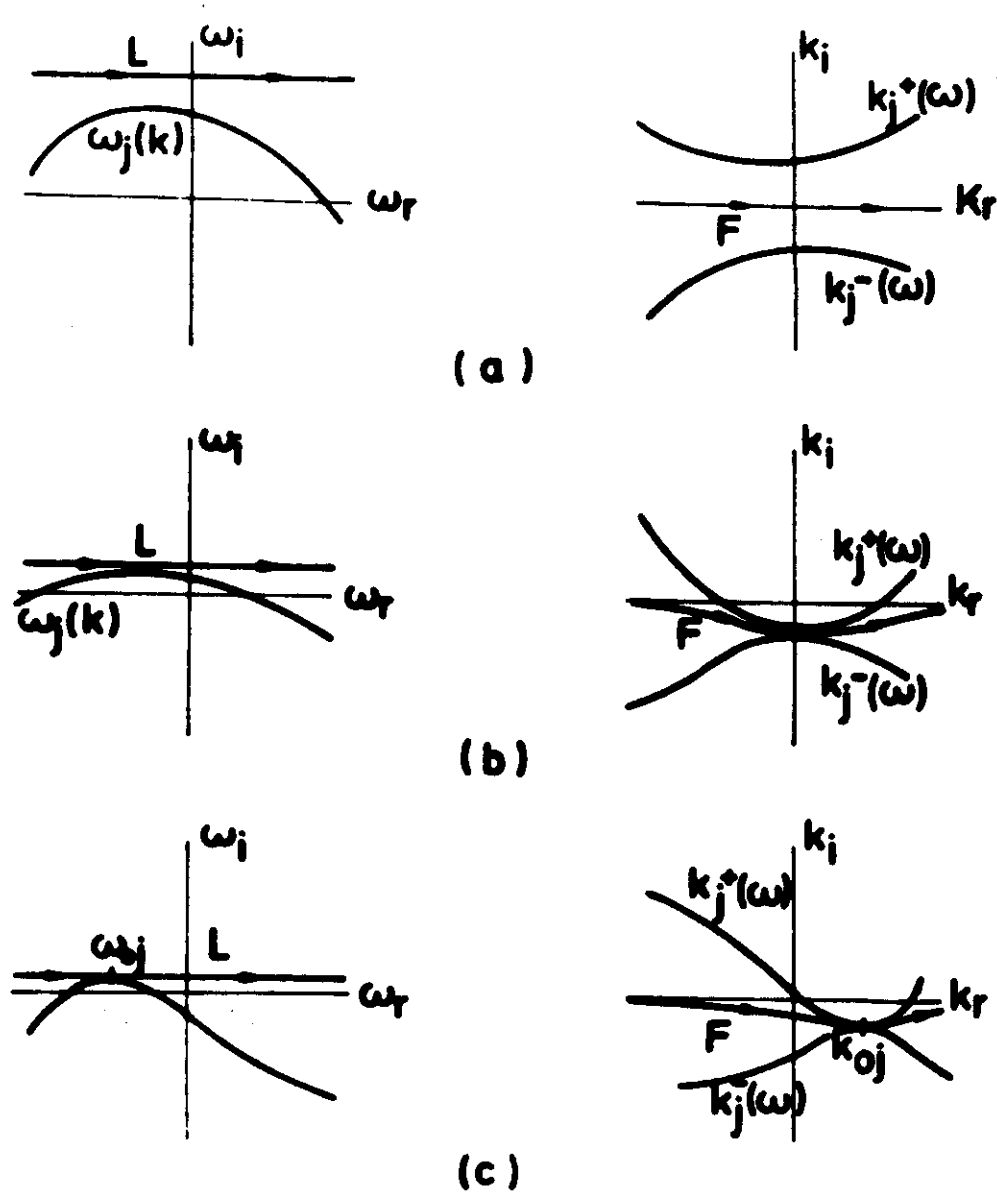


Figure 3. Locus of spatial branches $k_j^{+,-}(\omega)$ as L contour is displaced downward in complex ω -plane. (a), (b), and (c) describe different stages of pinching process.

As emphasized in a recent paper by Pierrehumbert [11], it may also happen that the two Riemann sheets of the branch point ω_{0j} pertain to spatial branches, say $k_j^+(\omega)$ and $k_j^-(\omega)$ located, for high enough L , in the same half k -plane. When the contour L is lowered, no pinching of the F contour can therefore occur. The corresponding branch point (ω_{0j}, k_{0j}) is not associated with an absolute growth rate. Presumably, the contour F cannot be deformed continuously to go through the saddle point along a path of steepest descent and the mode ω_{0j} does not appear in the response (12). An example of this type of behavior is given in section 3.2.

Thus a flow is convectively (absolutely) unstable when the branch points of $k(\omega)$, which pertain to spatial branches $k^+(\omega)$ and $k^-(\omega)$ originating from distinct halves of the k -plane, are located in the lower (upper) half ω -plane.

2.3. Spatial waves: the signalling problem in convectively unstable media.

Let us now consider the response of the flow to a simple monochromatic input of frequency ω_f located at $x=0$ and switched on at $t=0$. The initial state is assumed to be identically zero so that

$$D[-i\frac{\partial}{\partial x}, i\frac{\partial}{\partial t}; R]A(x, t) = \delta(x)H(t)e^{-i\omega_f t} \quad (17)$$

which, in the spectral domain, yields

$$A(k, \omega) = \frac{i}{D[k, \omega; R](\omega - \omega_f)} \quad (18)$$

The evaluation of the inverse Fourier transform in ω

$$A(k, t) = \frac{i}{2\pi} \int_L \frac{e^{-i\omega t}}{D[k, \omega; R](\omega - \omega_f)} d\omega \quad (19)$$

leads us, when $t > 0$, to distinguish several contributions to the response arising from the poles of the integrand in (19). The transient signal, due to switch-on, is associated with the zeroes of the dispersion relation $D[k, \omega; R]$, whereas the steady-state response is related to the simple pole at $\omega = \omega_f$. A straightforward residue calculation gives

$$A(k, t) = 2\sum_j \frac{\omega_j(k)e^{-i\omega_j(k)t}}{[\omega_j^2(k) - \omega_f^2](\partial D/\partial \omega)[k, \omega_j(k); R]} + \frac{e^{-i\omega_f t}}{D[k, \omega_f; R]} \quad (20)$$

and the Fourier transform of (20) with respect to k reads

$$\begin{aligned}
 A(x,t) = & \frac{1}{\pi} \sum_j \int_{-\infty}^{+\infty} \frac{\omega_j(k) e^{i[kx - \omega_j(k)t]} dk}{[\omega_j^2(k) - \omega_f^2] (\partial D/\partial \omega) [k, \omega_j(k); R]} \\
 & + \frac{e^{-i\omega_f t}}{2\pi} \int_{-\infty}^{+\infty} \frac{e^{ikx}}{D[k, \omega_f; R]} dk.
 \end{aligned} \tag{21}$$

As $t \rightarrow \infty$, the first term's asymptotics can be obtained via the method of steepest descent, in exactly the same manner as in section 2.1. The second term is calculated by closing the contour F in the upper (lower) half k -plane for $x > 0$ ($x < 0$). Residue contributions arise from the zeroes $k_j^+(\omega_f)$ and $k_j^-(\omega_f)$ of the dispersion relation at a fixed real frequency ω_f . These are precisely the spatial branches encountered in many calculations. One arrives at the final result:

$$\begin{aligned}
 A(x,t) \sim & \left(\frac{2}{\pi}\right)^{1/2} e^{-i\pi/4} \cdot \\
 & \cdot \sum_j \frac{\omega_j(k_j^*) e^{i[k_j^* x - \omega_j(k_j^*) t]}}{[\omega_j^2(k_j^*) - \omega_f^2] (\partial D/\partial \omega) [k_j^*, \omega_j(k_j^*); R] [d^2 \omega_j / dk^2 (k_j^*) t]^{1/2}} \\
 & + i \sum_j \frac{e^{i[k_j^+(\omega_f) x - \omega_f t]}}{(\partial D/\partial k) [k_j^+(\omega_f), \omega_f; R]} H(x) - i \sum_j \frac{e^{i[k_j^-(\omega_f) x - \omega_f t]}}{(\partial D/\partial k) [k_j^-(\omega_f), \omega_f; R]} H(-x),
 \end{aligned} \tag{22}$$

where the wavenumbers k_j^* are given, along the ray x/t , by equation (11) and H denotes the Heaviside unit step function. The solution is composed of a switch-on transient of the same qualitative form as the Green's function (12) and a "steady-state" response arising from forcing the flow at the frequency ω_f . The latter part takes the form of *spatially* growing and/or decaying waves located on either side of the source. The spatial branches $k_j^+(\omega_f)$ and $k_j^-(\omega_f)$ have unambiguously been assigned to the domains $x > 0$ and $x < 0$, respectively. This stems from the fact that they originate, for high enough L , from the upper and lower half k -plane respectively, as discussed in section 2.2.

If the flow is absolutely unstable, the transient contribution will progressively overwhelm the "steady-state" response at all spatial locations, thereby making the signalling problem meaningless. In a sense, spatially-growing waves are pathologically unstable to any kind of perturbations. However, if the flow is convectively unstable, transients will gradually move away from the source, leaving a genuinely observable steady-state signal. Spatially-growing waves are only relevant in convectively unstable physical systems.

3. APPLICATION TO AMPLITUDE EVOLUTION MODELS

In the following, the general concepts introduced in the previous sections are applied to three specific amplitude evolution models which commonly arise in the study of hydrodynamic instabilities.

3.1 The linearized Ginzburg-Landau equation

Perturbation analysis of fluid dynamical systems close to marginal stability at a finite wavenumber often lead to the Ginzburg-Landau

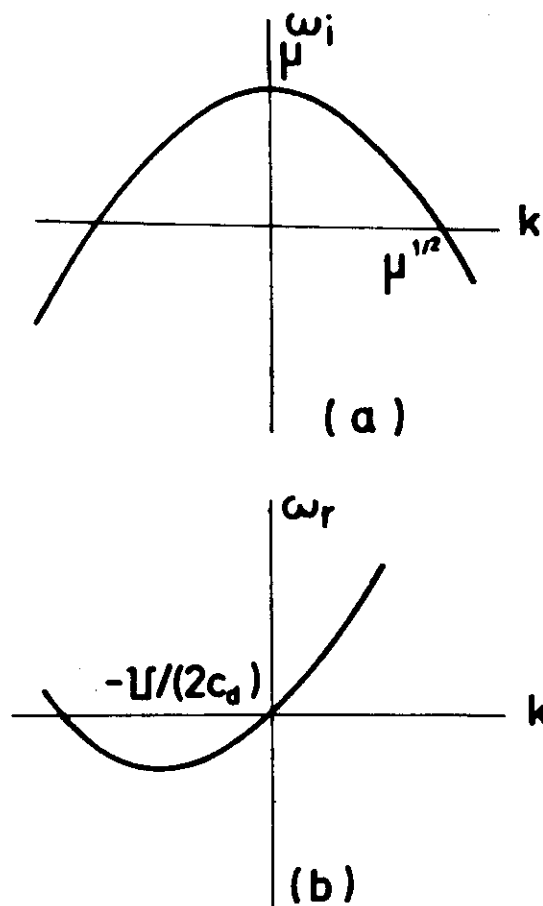


Figure 4. Temporal mode of the Ginzburg-Landau equation: (a) Temporal growth rate ω_i versus real wavenumber k ; (b) ω_r versus real wavenumber k .

equation. In the particular context of Rayleigh-Bénard convection, this model bears the name of Newell-Whitehead [12] and Segel [13]. In plane Poiseuille flow, it has been studied and derived by Stewartson & Stuart [14]. If $A(x,t)$ denotes the complex amplitude function of a wavepacket, the linear operator D takes the particular form

$$\frac{\partial A}{\partial t} + U \frac{\partial A}{\partial x} - \mu A - (1 + ic_d) \frac{\partial^2 A}{\partial x^2} = 0, \quad (23)$$

where U , μ and c_d are given real parameters. The parameter μ measures the "degree of supercriticality", i.e. how deep inside the unstable domain the system is. The constant c_d is calculated once and for all in a given flow situation, and U is a velocity which, when nonzero, breaks the reflectional symmetry $x \rightarrow -x$. The dispersion relation gives rise to a single temporal mode (Figures 4a,b)

$$\omega(k) = i\mu + Uk + (c_d - 1)k^2, \quad (24)$$

of group velocity

$$\frac{d\omega}{dk} = U + 2(c_d - 1)k. \quad (25)$$

When $\mu < 0$, the system is stable. When $\mu > 0$, it is unstable, the maximum growth rate $\omega_i(k_{\max}) = \mu$ occurring at $k_{\max} = 0$. The branch point of $k(\omega)$ is obtained by solving for $(d\omega/dk)(k_0) = 0$, which immediately yields

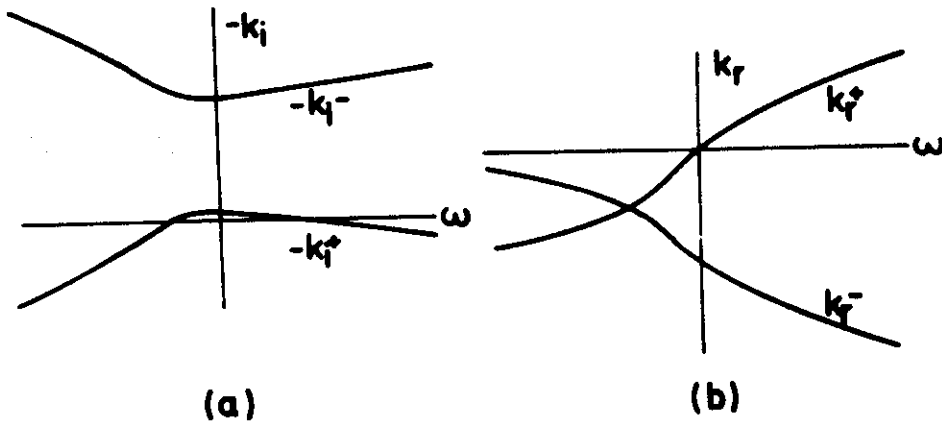


Figure 5. Spatial branches of the Ginzburg-Landau equation: (a) Spatial growth rate $(-k_i)$ versus real frequency ω ; (b) k_r versus real frequency ω . The velocity U is such that $U > 2[\mu(1 + c_d^2)]^{1/2}$.

$$k_0 = -\frac{U}{2(c_d - i)}; \quad \omega_0 = iU - \frac{U^2}{4(c_d - i)}. \quad (26a, b)$$

The temporal mode may then be rewritten in the convenient form

$$\omega(k) - \omega_0 = (c_d - i)(k - k_0)^2, \quad (27)$$

thereby clearly displaying the fact that the singularity is an algebraic branch point of order two. For a given value of ω , there exists two spatial branches (Figure 5a,b) given by

$$k^{+,-}(\omega) = k_0 \pm \left(\frac{\omega - \omega_0}{c_d - i}\right)^{1/2} \quad (28)$$

As the complex frequency $\omega = \omega_r + i\omega_{iL}$ varies along the straight line contour L , at the height ω_{iL} , the spatial branches are restricted to the hyperbola

$$(1 + c_d^2)(k_i - k_{0,i})^2 - (k_r - c_d k_{0,r}) = \omega_{iL} - \omega_{0,i}, \quad (29)$$

as sketched in Figure 6a,b. As ω_{iL} becomes sufficiently large, the two spatial branches $k^+(\omega)$ and $k^-(\omega)$ belong to distinct halves of the k -plane, and (k_0, ω_0) is a genuine singular point for the determination of absolute or convective instability (see section 2.2).

The absolute growth rate is equal to the imaginary part of (26b),

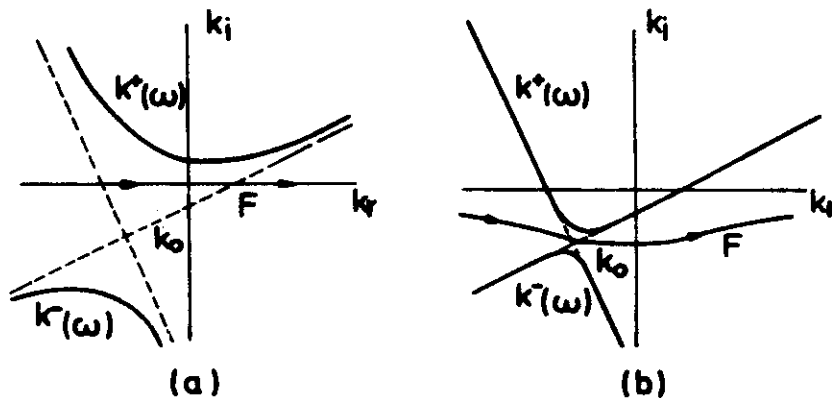


Figure 6. Locus of spatial branches as $\omega_{0,i}$ is decreased: (a) and (b) describe different stages of pinching process for the Ginzburg-Landau equation.

namely

$$\omega_i(k_0) = \omega_{0,i} = \mu - \frac{U^2}{4(1+c_d^2)} \quad (30)$$

When $|U| < 2\mu^{1/2}(1+c_d^2)^{1/2}$, the absolute growth rate is positive and the system is absolutely unstable. When $|U| > 2\mu^{1/2}(1+c_d^2)^{1/2}$, it is negative and the system is convectively unstable.

The Green's function $G(x,t)$ is given by (10) with $\omega(k)$ specified by (27), so that

$$G(x,t) = \frac{1}{2\pi} e^{-i\omega_0 t} \int_{-\infty}^{+\infty} e^{i[kx - (c_d - i)(k-k_0)^2 t]} dk \quad (31)$$

This integral can be evaluated exactly by a straightforward change of variable to give the closed form solution

$$G(x,t) = \frac{1}{2} (\pi t)^{-1/2} (1 + ic_d)^{-1/2} \exp[i(k_0 x - \omega_0 t) - \frac{x^2}{4(1 + ic_d)t}] \quad (32)$$

The method of steepest descent would yield in this case the exact result (32) by application of equation (12). The response to an impulse takes the form of a wavepacket which displays all of the main characteristics of the general case as discussed in section 2.1. The peak grows at the maximum growth rate μ along the ray $x/t = U$. The edges of the wavepacket, where the growth rate is equal to zero, move at the velocities $U \pm 2(1+c_d^2)^{1/2}\mu^{1/2}$. At a fixed x location, the asymptotic temporal growth rate is, as $t \rightarrow \infty$, $\omega_{0,i}$, the absolute growth rate at $k = k_0$. An alternate expression for (32) is

$$G(x,t) = \frac{1}{2} (\pi t)^{-1/2} (1 + ic_d)^{-1/2} \exp[\mu t - \frac{(x-Ut)^2}{4(1+ic_d)t}] \quad (33)$$

The reader may apply to this result all the definitions and concepts introduced in section 2, to recover the main conclusions regarding the stability or instability of the system. The parameter μ is seen to control the peak growth rate while the parameter U controls the absolute growth rate. Different responses are illustrated in Figure 7.

In the convectively unstable case, the solution of the signalling problem satisfies (22), the spatially-evolving waves issuing from the monochromatic source having characteristics displayed on Figures 5a,b.

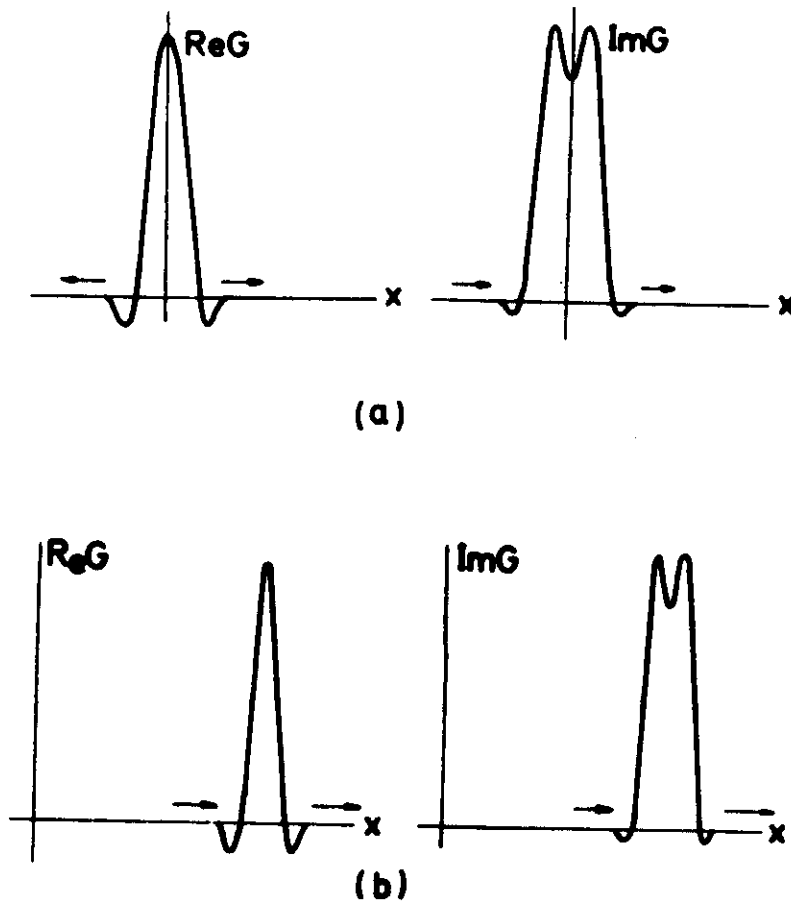


Figure 7. Green's function of the Ginzburg-Landau equation: (a) absolutely unstable case; (b) convectively unstable case.

3.2. The linear Klein-Gordon equation

The cubic nonlinear Klein-Gordon equation commonly arises in inviscid marginal stability analysis such as the baroclinic instability of a quasi-geostrophic two-layer model on the β plane [15], the Kelvin-Helmoltz instability of two layers of immiscible fluids [16], or the buckling of thin shells [17]. When linearized, the model takes the form

$$\left(\frac{\partial}{\partial t} + U\frac{\partial}{\partial x}\right)^2 A - \frac{\partial^2 A}{\partial x^2} - \mu A = 0, \quad (34)$$

and the dispersion relation in Fourier space reduces to

$$D[k, \omega] \equiv -(\omega - Uk)^2 + k^2 - \mu = 0. \quad (35)$$

There are two temporal modes (figures 8a,b)

$$\omega_{1,2}(k) = Uk \pm (k^2 - \mu)^{1/2}, \quad (36)$$

of group velocity

$$\frac{d\omega_{1,2}}{dk} = U \pm k(k^2 - \mu)^{-1/2}. \quad (37)$$

When $\mu < 0$, the system is neutrally stable, in the sense that $\omega_1(k)$ and $\omega_2(k)$ are purely real. When $\mu > 0$, the flow is unstable to wavenumbers in the range $|k| < \mu^{1/2}$. The value of U determines, as before, the character of the instability.

In the range $|U| < 1$, the two spatial branches are given by

$$k^\pm(\omega) = -\frac{\omega U}{1 - U^2} \pm \frac{1}{1 - U^2}[\omega^2 + \mu(1 - U^2)]^{1/2}, \quad (38)$$

and the branch points of $k(\omega)$ are located on the imaginary axis at

$$\omega_0 = \pm i[\mu(1 - U^2)]^{1/2}; \quad k_0 = \pm iU[\mu/(1 - U^2)]^{1/2}. \quad (39)$$

As in the previous example, one may check that, for ω_{iL} sufficiently large, the spatial branches are restricted to the upper and lower half k -plane respectively. Pinching first takes place at $\omega_0 = i[\mu(1 - U^2)]^{1/2}$ and $k_0 = -iU[\mu/(1 - U^2)]^{1/2}$, as ω_{iL} is gradually decreased (figures 9a,b,c). The absolute growth rate is positive and it must be concluded that the instability is absolute.

For parameter values such that $|U| > 1$, the spatial branches can be more conveniently written as

$$k_{1,2}^+ = \frac{\omega U}{U^2 - 1} \pm \frac{1}{U^2 - 1}[\omega^2 - \mu(U^2 - 1)]^{1/2}, \quad (40)$$

and the branch points at

$$\omega_0 = \pm[\mu(U^2 - 1)]^{1/2}, \quad k_0 = \pm U[\mu/(U^2 - 1)]^{1/2} \quad (41)$$

are confined to the real ω -axis. At large values of ω_{iL} , the spatial branches are located in the *same* half k -plane (upper half k -plane if $U > 1$, lower half k -plane if $U < -1$). As ω_{iL} is decreased to zero so that the L contour touches the branch points on the real ω -axis, the spatial roots "collide" *without* pinching the F contour (see Figures 10a, b, c). The branch points at $\omega_0 = \pm\{\mu(U^2 - 1)\}^{1/2}$ therefore do not contribute to an absolute growth rate which, at any rate, would be zero. The instability is convective.

The Green's function can be calculated exactly [18,16], by inverting $G(k, \omega) = 1/D(k, \omega)$, with $D(k, \omega)$ given by (35). For definitiveness, it is assumed that $|U| < 1$, but the same final result holds when $|U| > 1$. Instead of performing the ω -integration first (see section 2.1) we choose here, as an illustration, to first evaluate

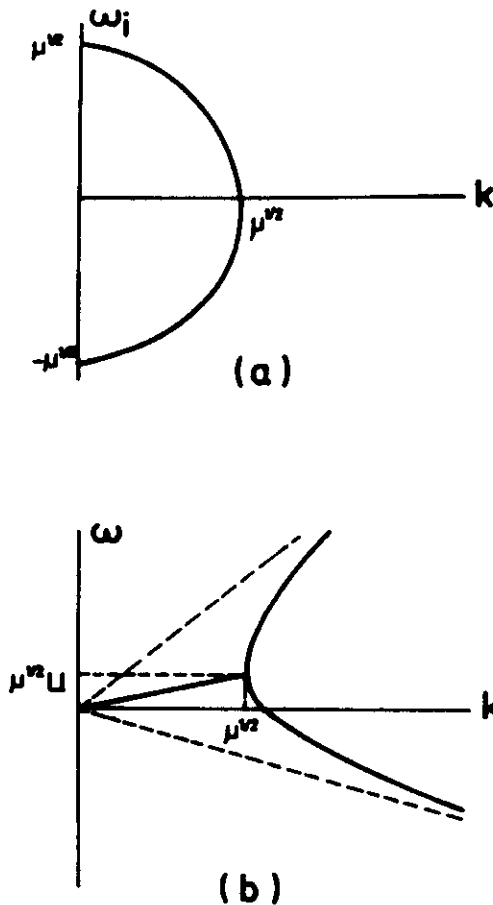


Figure 8. Temporal modes of the Klein-Gordon equation: (a) Temporal growth rate ω_i versus real wavenumber k ; (b) ω_r versus real wavenumber k .

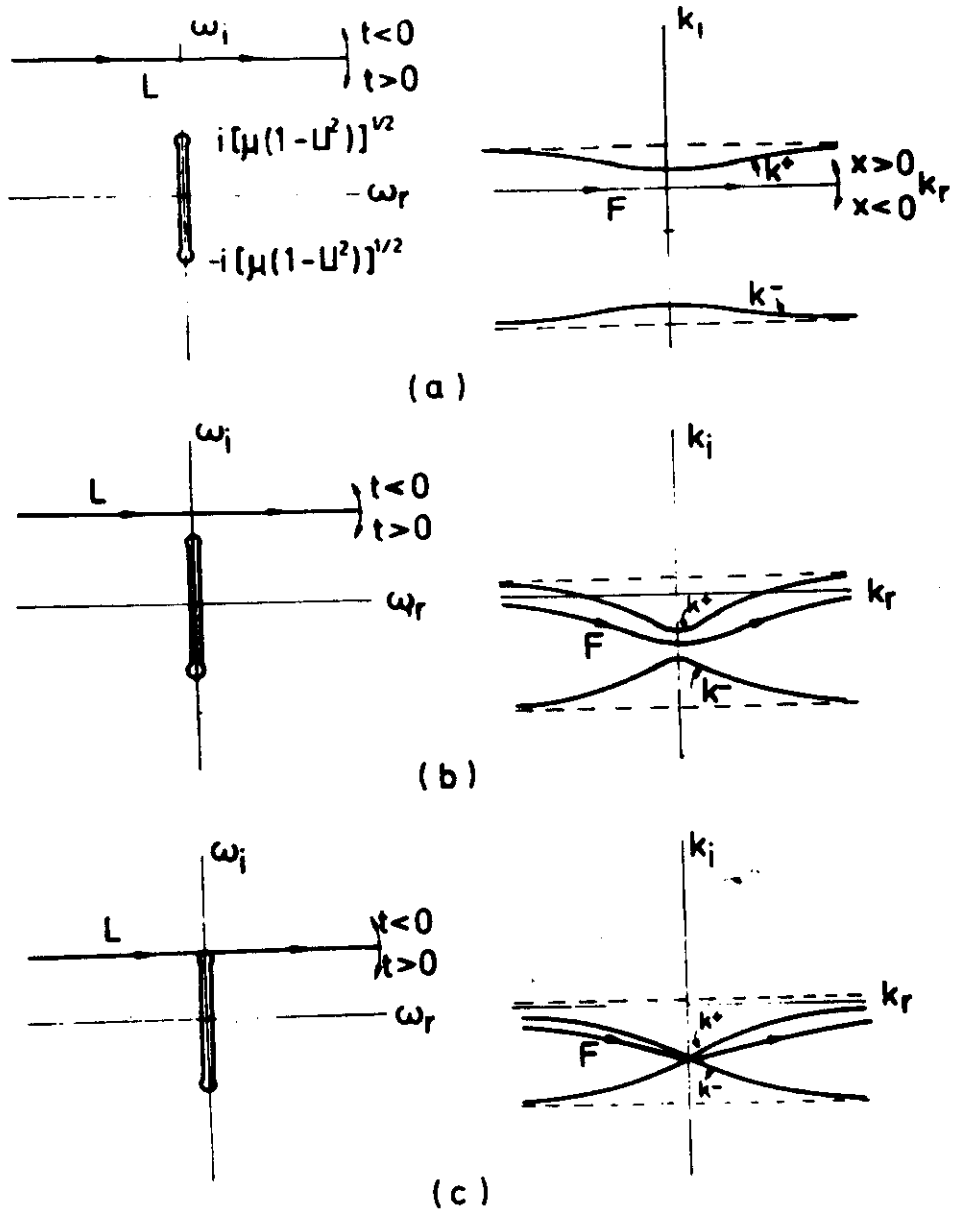


Figure 9. Locus of spatial branches in the k -plane, as ω_{iL} is decreased: (a), (b) and (c) describe different stages of pinching process in the Klein-Gordon equation. The velocity U is such that $|U| < 1$. Flow is absolutely unstable.

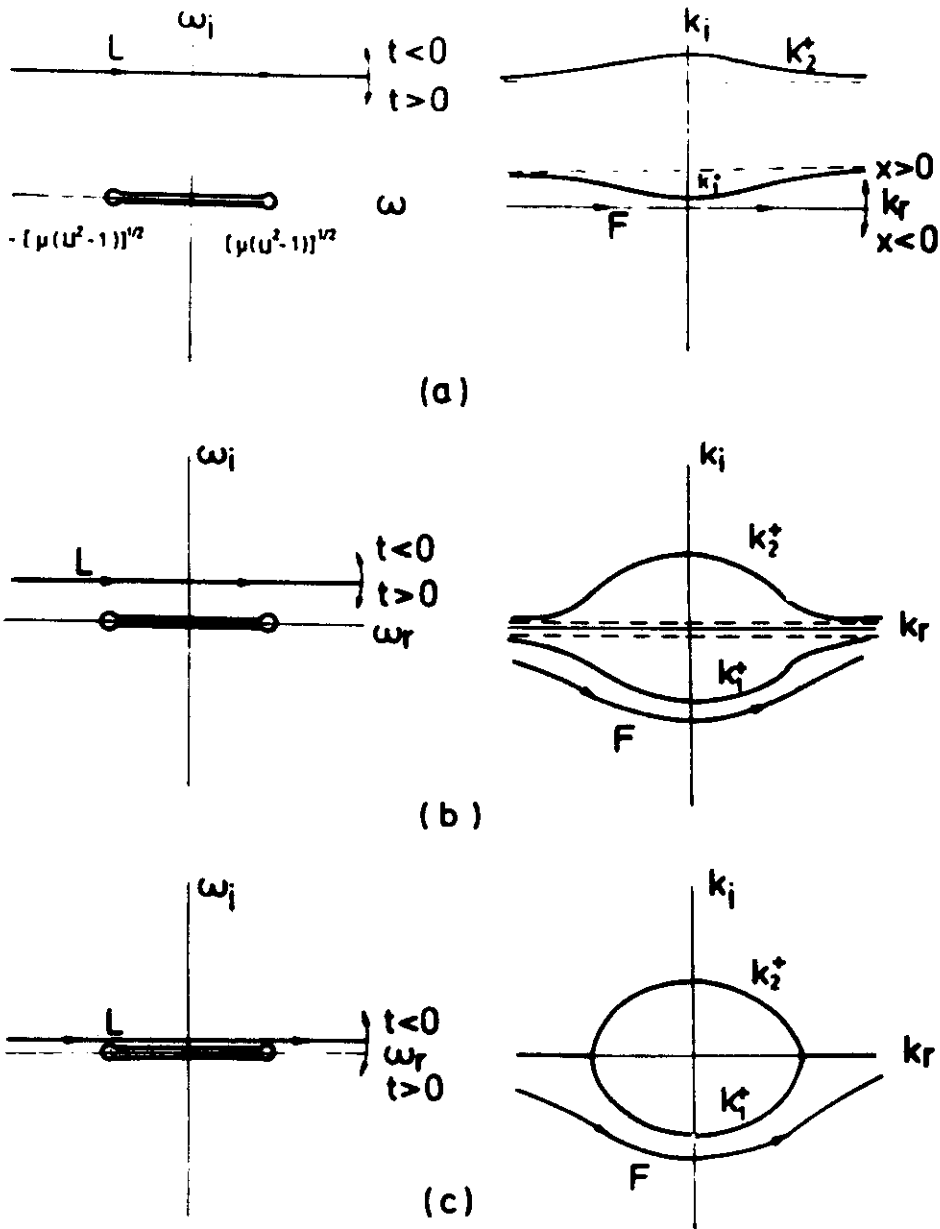


Figure 10. Same as figure 9, when $|U| > 1$. Flow is convectively unstable. Note absence of pinching of F contour by spatial branches.

the integral over all wavenumbers, namely

$$G(x, \omega) = \frac{1}{2\pi} \int_{-\infty}^{+\infty} \frac{e^{ikx}}{(1-U^2)[k-k^+(\omega)][k-k^-(\omega)]} dk. \quad (42)$$

There are two simple poles $k = k^{\pm}(\omega)$ located on either side of the real k axis when $|U| < 1$ (recall the previous discussion). Closing the contours as indicated in Figure 9a, one obtains the residue contributions

$$G(x, \omega) = \frac{i}{2(1-U^2)} \left[H(x) \frac{e^{ik^+(\omega)x}}{K(\omega)} + H(-x) \frac{e^{ik^-(\omega)x}}{K(\omega)} \right] \quad (43)$$

with

$$K(\omega) = \frac{1}{1-U^2} [\omega^2 + \mu(1-U^2)]^{1/2}, \quad (44)$$

and $k^{\pm}(\omega)$ given by (38).

There remains to evaluate the inverse transform with respect to ω

$$G(x, t) = \frac{i}{4\pi(1-U^2)} [H(x)I^+ + H(-x)I^-], \quad (45)$$

where

$$I^{\pm} \equiv \int_L \frac{\exp\{i[k^{\pm}(\omega)x - \omega t]\}}{K(\omega)} d\omega. \quad (46)$$

The contour L is chosen to be above the branch cut (Figure 9) linking the branch points at $\omega_0 = \pm i[\mu(1-U^2)]^{1/2}$. An elementary examination of the real part of each exponent indicates that the contour should be closed from above when $t^2 - (x-Ut)^2 < 0$. Cauchy's theorem then yields $G(x, t) = 0$. In the range $t^2 - (x-Ut)^2 > 0$, it is convenient to introduce the notation $U = \tanh\theta$ and the parameters ξ and θ such that

$$x - Ut = \xi \sinh\theta, \quad t = \xi \cosh\theta, \quad (47)$$

conversely,

$$\xi = [t^2 - (x-Ut)^2]^{1/2}, \quad \tanh\theta = (x-Ut)/t. \quad (48)$$

The integral I^+ may then be written as

$$I^+ = \int_L \frac{\exp\{i\xi[-\omega \cosh \alpha \cosh(\theta + \alpha) + \sinh(\theta + \alpha)((\omega \cosh \alpha)^2 + \mu)^{1/2}]\}}{\cosh \alpha [(\omega \cosh \alpha)^2 + \mu]^{1/2}} d\omega. \quad (49)$$

A closed form solution can then be obtained by deforming L around the branch cut. A parametric representation of ω along the branch cut is given by

$$\omega \cosh \alpha = i\mu^{1/2} \cos \psi, \quad -\pi < \psi < +\pi \quad (50)$$

with

$$[(\omega \cosh \alpha)^2 + \mu]^{1/2} = \mu^{1/2} \sin \psi \quad (51)$$

on both sides of the cut (Figure 9). The integral I^+ is then rearranged as

$$I^+ = -\frac{i}{\cosh^2 \alpha} \int_{-\pi}^{+\pi} \exp[\mu^{1/2} \xi \cos(\psi - i(\theta + \alpha))] d\psi. \quad (52)$$

The above integral is zero around the contour C sketched in Figure 11. Evaluation of the contributions along the 4 segments making up C leads to the final expression

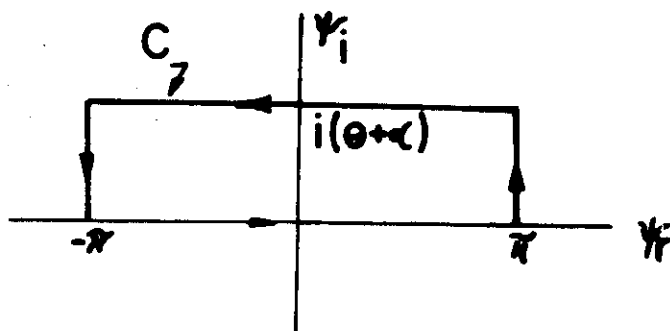


Figure 11. Contour C used to derive (53) from (52).

$$I^+ = -\frac{2i}{\cosh^2 \alpha} \int_0^\pi \exp[\mu^{1/2} \xi \cos \psi] d\psi. \quad (53)$$

The integral representation of the modified Bessel function I_0 is recognized [19] so that

$$I^+ = -\frac{2\pi i}{\cosh^2 \alpha} I_0(\mu^{1/2} \xi). \quad (54)$$

Bearing in mind that $I^- = I^+$, the Green's function pertaining to the Klein-Gordon equation then reduces to

$$G(x, t) = \frac{1}{2} I_0[\mu^{1/2}(t^2 - (x - Ut)^2)^{1/2}] H(t^2 - (x - Ut)^2). \quad (55)$$

The above result remains valid when $|U| > 1$.

In the long-time limit, one may use the asymptotic expansion of I_0 to arrive at the result one would obtain from a steepest descent calculation, namely,

$$G(x, t) \sim \frac{1}{2(2\pi)^{1/2}} \frac{\exp[\mu^{1/2}(t^2 - (x - Ut)^2)^{1/2}]}{\mu^{1/4}(t^2 - (x - Ut)^2)^{1/4}} H(t^2 - (x - Ut)^2). \quad (56)$$

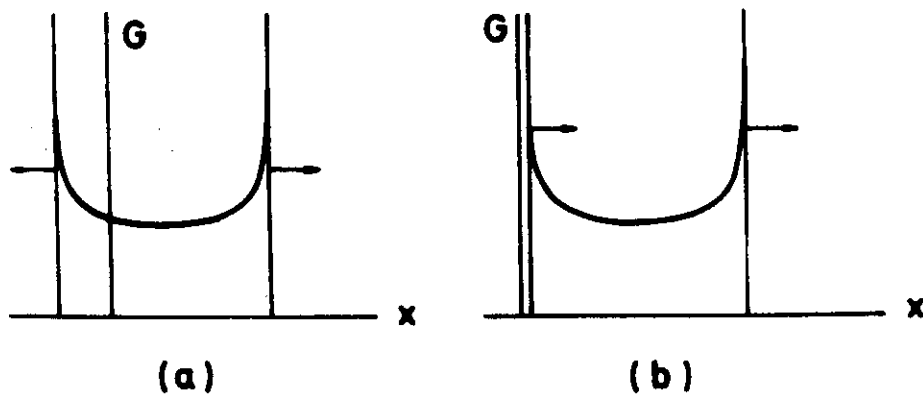


Figure 12. Green's function of the Klein-Gordon equation: (a) absolutely unstable case; (b) convectively unstable case.

The peak of the packet experiences the maximum growth rate $\mu^{1/2}$ and travels along the ray $x/t = U$. The edges move at the respective velocities $U \pm 1$. The absolute growth rate is $[\mu(1 - U^2)]^{1/2}$ when $|U| < 1$ and zero when $|U| > 1$. The impulse response is sketched in Figure 12.

In the range $|U| > 1$, spatially-developing waves can be generated with the stability characteristics sketched in Figures 13a,b. Note that both waves develop downstream of the source when $U > 1$, in agreement with a previous discussion on spatial branches. The steady-state response is of the form (22) with no terms multiplying $H(-x)$ when $U > 1$. To emphasize this feature, the spatial branches have been renamed k_1^+ and k_2^+ as in (40).

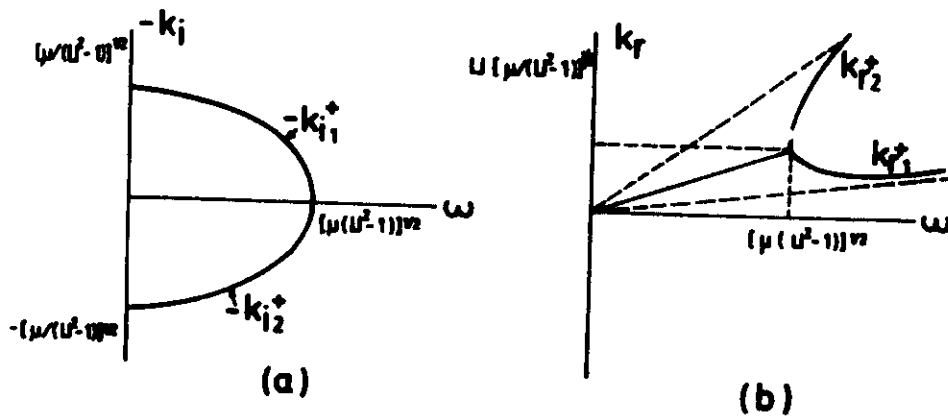


Figure 13. Spatial branches of the Klein-Gordon equation: (a) Spatial growth rate ($-k_i$) versus real frequency ω ; (b) k_r versus real frequency ω . The velocity U is such that $U > 1$.

3.3. A long wavelength evolution equation

As a last example, we consider a long wavelength evolution equation pertinent to the Kelvin-Helmholtz instability in bounded mixing layers [6]. The model will serve to illustrate the type of technique which may be applied when the dispersion relation contains $|k|$ terms and is therefore not analytic. When a general forcing term $s(x,t)$ is present, the linearized version of the model reads

$$D_a \left[-i \frac{\partial}{\partial x}, i \frac{\partial}{\partial t} \right] a(x,t) \equiv \frac{1}{\pi x} * \left(\frac{\partial}{\partial t} + U \frac{\partial}{\partial x} \right) a + \mu \frac{\partial a}{\partial x} + \frac{\partial^2 a}{\partial x^2} = s(x,t), \tag{57}$$

where $a(x,t)$ and $s(x,t)$ are real, and

$$f * h = \int_{-\infty}^{+\infty} f(x - \epsilon) h(\epsilon) d\epsilon \quad (58)$$

is the spatial convolution of the functions f and h . The dispersion relation in this case takes the form

$$D_a[k, \omega] \equiv -sqnk(\omega - Uk) + ik(\mu - k^2) = 0, \quad (59)$$

and there exists a single temporal mode characterized by

$$\omega_a(k) = Uk + i|k|(\mu - k^2). \quad (60)$$

The system becomes unstable when $\mu > 0$, the maximum growth rate $\omega_i(k_{\max}) = 2(\mu/3)^{3/2}$ being reached at $k_{\max} = (\mu/3)^{1/2}$, as shown in Figures 14a,b.

To facilitate the interpretation of $|k|$ in the complex plane, it is convenient to associate with the *real* signal $a(x,t)$, the complex "*analytic signal*" $A(x,t)$ (see, for instance, [20]) defined by

$$A(x,t) = [\delta(x) + i/(\pi x)] * a(x,t); \quad (61a,b)$$

$$a(x,t) = \text{Re}A(x,t).$$

The symbol Re indicates the real part of a complex quantity. If $a(k,t)$ and $A(k,t)$ are the spatial Fourier transforms of $a(x,t)$ and $A(x,t)$ respectively, relations (61a,b) become, in wavenumber space

$$A(k,t) = 2H(k)a(k,t); \quad (62a,b)$$

$$a(k,t) = \frac{1}{2} [A(k,t) + \bar{A}(-k,t)],$$

a bar denoting the complex conjugate. Thus, the spectrum of $A(x,t)$ is nothing but the restriction of the spectrum of $a(x,t)$ to *positive* wavenumbers only. Hence, the analytic signal $A(x,t)$ is merely the extension to arbitrary waveforms of the complex notation which, in linear systems, relates a monochromatic real signal $a(x) = \cos k_0 x$ and its complex equivalent $A(x) = e^{ik_0 x}$. Once $A(x,t)$ is known, the real signal $a(x,t)$ can be obtained by taking the real part $a(x,t) = \text{Re}A(x,t)$, as required by (61b). All the calculations can therefore be performed on $A(x,t)$ which is easily shown to satisfy

$$D \left[-i \frac{\partial}{\partial x}, i \frac{\partial}{\partial t} \right] A(x,t) \equiv -i \left(\frac{\partial A}{\partial t} + U \frac{\partial A}{\partial x} \right) + \mu \frac{\partial A}{\partial x} + \frac{\partial^3 A}{\partial x^3} = S(x,t). \quad (63)$$

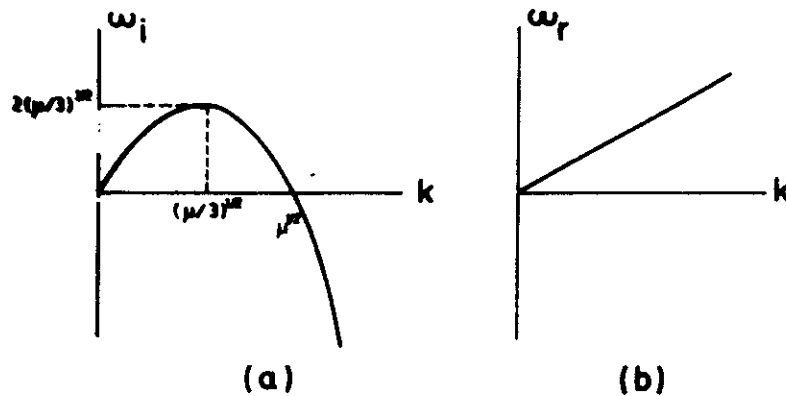


Figure 14. Temporal mode of the long wavelength equation (57): (a) Temporal growth rate ω_i versus real wavenumber k ; (b) ω_r versus real wavenumber k .

The function $S(x,t)$ is the analytic signal corresponding to $s(x,t)$, as defined in the pair (61a,b). The new dispersion relation

$$D(k,\omega) \equiv -(\omega - Uk) + ik(\mu - k^2) = 0, \quad (64)$$

is analytic in k . It has been obtained from (59) by simply choosing $\text{sgn}k = +1$. The inverse of $D(k,\omega)$ defines the operator acting on the analytic signal $A(x,t)$ in (63). Since the spectrum of A is identically zero for $k < 0$, the general formalism developed in section 2 holds, provided the contour F is initially taken to be the *positive* real axis instead of the entire real line. The study of the trajectories of the poles in the integrand can be *restricted to the half-plane* $k_r > 0$ and its corresponding image in the ω -plane. We note that (63) is the linearized form of the Korteweg-deVries equation with complex coefficients. The temporal mode is given by

$$\omega(k) = Uk + ik(\mu - k^2), \quad (65)$$

which can be compared with (60). The branch point of $k(\omega)$, obtained by solving for $(d\omega/dk)(k_0) = 0$, is located at

$$k_0 = [(\mu - iU)/3]^{1/2}, \quad \omega_0 = 2ik_0^3, \quad (66)$$

with $k_{0r} > 0$. At each value of ω , there are in general 3 spatial branches, only two of which are located in the half-plane $k_r > 0$. The branch point (66) involves genuine pinching of the F contour by branches $k^+(\omega)$ and $k^-(\omega)$ originating from distinct sectors $k_i > 0$ and $k_i < 0$ as L is lowered. The absolute growth rate ω_{0i} becomes zero when $|U| = \mu/3$. The system is therefore absolutely (convectively) unstable when $|U| < \mu/3$ ($|U| > \mu/3$).

The Green's function $g = \text{Re}G$ is calculated by solving for

$$D \left[-i \frac{\partial}{\partial x}, i \frac{\partial}{\partial t} \right] G = \left(\delta(x) + \frac{i}{\pi x} \right) \delta(t), \quad (67)$$

equivalently,

$$G(k, \omega) = 2H(k)/D(k, \omega). \quad (68)$$

A straightforward residue evaluation in the complex ω -plane leads to the wavepacket integral

$$G(x, t) = -\frac{i}{\pi} \int_0^{+\infty} \frac{e^{i[kx - \omega(k)t]}}{(\partial D / \partial \omega)[k, \omega(k)]} dk, \quad (69)$$

which should be compared with the general formula (10). We note that the k -integral is limited to the range $0 < k < +\infty$. The application of the method of steepest descent involves a stationary point k^* such that $(d\omega/dk)(k^*) = x/t$, as well as a boundary point $k = 0$. Since in the particular example considered here $\omega_1(0) = 0$, the saddle point contribution at k^* will dominate the response inside the wavepacket. Rather than pursuing this argument, we choose to derive an exact representation of $G(x, t)$ when the dispersion relation $D[k, \omega]$ is given by (64). The wavepacket integral then reduces to

$$G(x, t) = \frac{i}{\pi} \int_0^{+\infty} \exp[ik(x - Ut) + k(\mu - k^2)t] dk. \quad (70)$$

Upon making the change of variable $k = \tau/(3t)^{1/3}$, $G(x, t)$ can be recast as

$$G(x, t) = \frac{i}{\pi(3t)^{1/3}} \int_0^{+\infty} \exp(-\tau^3/3 + (3t)^{-1/3}[\mu t + i(x - Ut)]\tau) d\tau, \quad (71)$$

which involves the integral representation of the function $\text{Hi}(z)$ [19]. The real Green's function takes the following final expression:

$$g(x, t) = (3t)^{-1/3} \text{Re} \left\{ i \text{Hi} \left[\frac{\mu t + i(x - Ut)}{(3t)^{1/3}} \right] \right\}. \quad (72)$$

The asymptotic expansion of $\text{Hi}(z)$ as $|z| \rightarrow \infty$ leads to the same results as the method of steepest descent, namely

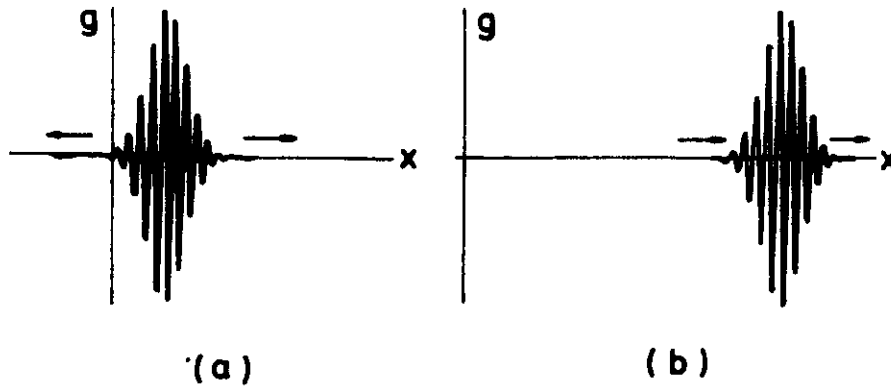


Figure 15. Green's function of the long wavelength equation (57): (a) absolutely unstable case; (b) convectively unstable case.

$$g(x,t) \sim \frac{1}{\pi^{1/2}(3t)^{1/4}} \operatorname{Re} \left[\frac{i}{[\mu t + i(x-Ut)]^{1/4}} \cdot \exp\left\{ \frac{2}{3} \frac{[\mu t + i(x-Ut)]^{3/2}}{(3t)^{1/2}} \right\} \right] \quad (73)$$

when $|(x-Ut)/t| < \mu/3$,

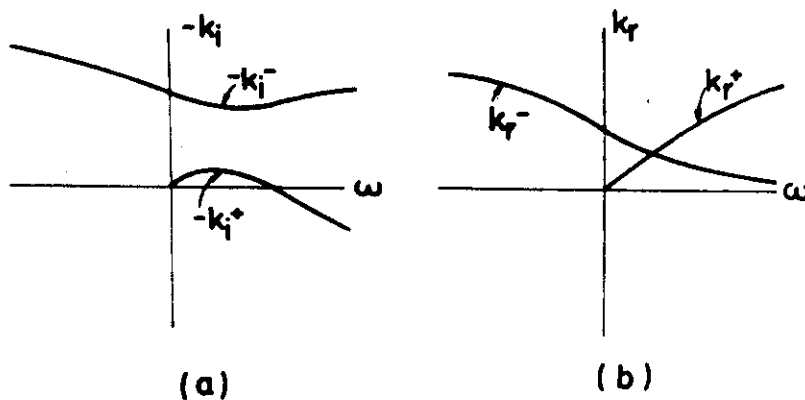


Figure 16. Spatial branches of the long wavelength equation (57): (a) spatial growth rate ($-k_i$) versus real frequency ω ; (b) k_r versus real frequency ω . The velocity U is such that $U > \mu\sqrt{3}$.

and

$$g(x,t) \sim \text{Re} \left[\frac{-i}{\pi[\mu t + i(x-Ut)]} \right], \text{ when } |(x-Ut)/t| > \mu\sqrt{3}. \quad (74)$$

The edges of the wavepacket move at the respective velocities $U \pm \mu\sqrt{3}$, and the critical values $U = \pm\mu\sqrt{3}$ signal the transition from absolute to convective instability. Typical responses are shown in Figure 15.

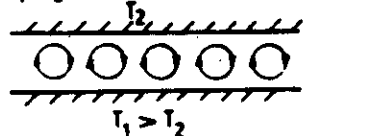
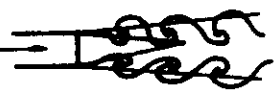
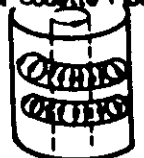
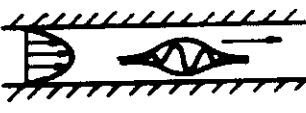
The characteristics of spatially-evolving waves are sketched in Figure 16, when $|U| > \mu\sqrt{3}$.

4. APPLICATION TO HYDRODYNAMIC INSTABILITIES

In the sequel, we shall emphasize the physical implications of the previous mathematical development. Recall that two classes of unstable flows have been distinguished.

4.1. Convectively unstable flows

In convectively unstable systems, any initial disturbance is advected by the flow as it is amplified and the medium is ultimately left undisturbed. In this instance, solutions of the dispersion relation with ω real and k complex are physically relevant. They describe the spatial evolution of a periodic excitation applied at a fixed spatial location. As a rule, convectively unstable flows are extremely sensitive to external forcing. *Receptivity* issues therefore play a crucial role in determining the fate of infinitesimal disturbances. At the same time, intrusive measurements leave the flow relatively

Absolutely Unstable Flows	Convectively Unstable Flows
<p>Rayleigh-Bénard Convection</p> 	<p>Jets (2D or 3D)</p> 
<p>Taylor Couette Flow</p> 	<p>Plane Poiseuille Flow</p> 

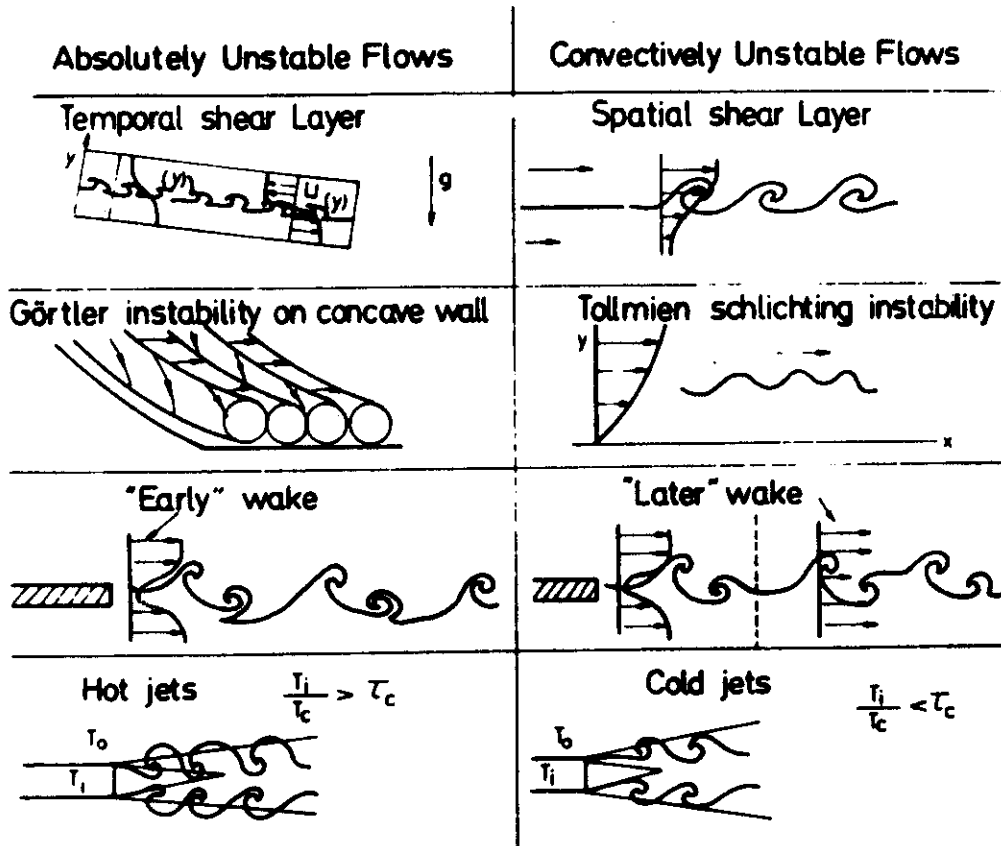


Figure 17. Tentative classification of common fluid flows into absolutely unstable flows and convectively unstable flows (see also [7]).

unaffected, provided no feedback loops or hydrodynamic resonances are willingly introduced (see later discussion). Examples of convectively unstable parallel flows are numerous in classical hydrodynamic stability theory, but few detailed calculations of the pertinent complex dispersion relations have been conducted. An incomplete, partially subjective, list is given in Figure 17. According to Huerre & Monkewitz [4], the family of parallel shear layer profiles $\bar{U}(y) = 1 + R \tanh y$ (\bar{U} : streamwise velocity, y : cross-stream direction, R : velocity ratio) is convectively unstable to *two-dimensional* disturbances whenever $R > 1.315$. Indeed, spatial stability theory [21,22] provides a consistent description of most instability waves in mixing layers generated downstream of a splitter plate. The *three-dimensional* wavepacket calculations of Balsa [23] further support the fact that such mixing layers are convectively unstable. A recent survey of experimental and theoretical results pertinent to shear layers has been made by Ho & Huerre [24]. Although no general results are presently available, there are very strong indications from the pioneering work of Gaster [25-28] that Tollmien-Schlichting waves in flat plate boundary layers are induced by a convective instability. It may be conjectured that plane Poiseuille flow is of a similar character. The dispersion relation associated with the Orr-Sommerfeld equation [29] is extremely rich in structure, which largely explains why no definite statement can be made regarding these viscous instabilities. Similarly, cold circular jets at low Mach numbers are probably convectively unstable and spatial instability theory [30] does represent the linear evolution of vortical disturbances in such a circular geometry. Note further that many of the above flows are far from being parallel. It is therefore implicitly assumed that the WKB formation can be applied successfully, the locally parallel basic flow being convectively unstable at all streamwise stations. Such an assumption does not necessarily take into account the effects of global pressure fluctuations, as opposed to *local vortical* fluctuations. For instance in shear layers, feedback loops between preferred downstream stations and the trailing-edge could make a locally convectively unstable medium to be globally absolutely unstable.

4.2. Absolutely unstable flows

In absolutely unstable systems, any infinitesimal disturbance contaminates the entire medium. As a result, intrusive measurements greatly affect the flow. Indeed, great care must be exercised in laboratory experiments, and non-intrusive techniques, such as Laser Doppler anemometry are often preferred. Spatial stability theory is irrelevant in absolutely unstable flows: any spatially-evolving wave is, in the course of time, overwhelmed by linear, temporally-growing fluctuations. Thus, in contrast with the previous class of instabilities, absolutely unstable flows tend to be less sensitive to infinitesimal external fluctuations. The behavior of the flow is *intrinsic* rather than *extrinsic*. Here again, one must rely on physical intuition to give fluid dynamical examples since no detailed

theoretical investigations of the dispersion relations have been undertaken in the complex plane. It is probably very safe to say that a horizontal fluid layer heated from below (see reference [31] for a review) does give rise to absolute instabilities. The centrifugal Görtler instability taking place in boundary layers along concave walls does not obviously fall in one class or another. Although a recent study by Hall [32] has shed considerable light on the spatial instability problem, the convective nature of the instability has not been established. The present author's personal prejudice would tend to guess that it is absolutely unstable. Before tackling this configuration, however, one would need to extend the formalism of section 2 to highly non-parallel flows for which no separation of variables is possible.

Finally, it is interesting to note that temporally evolving mixing layers can be obtained experimentally by tilting a tank filled with a stably stratified fluid [33]. These flows are such that $R > 1.315$ for the family of profiles $\bar{U}(y) = 1 + R \tanh y$; consequently, the medium is absolutely unstable [4] in contrast with shear layers generated downstream of a splitter plate. It is found that the temporal theory of Michalke [34] does predict the main features of the linear development of the Kelvin-Helmholtz vortices induced by the shear.

4.3. "Mixed flows" and Frequency Selection Mechanisms

There are also flow geometries which may give rise to a convective instability in one region of the flow and an absolute instability in another region. To our knowledge, this possibility has first been explored by Pierrehumbert [10] and Koch [35]. In such "mixed" flows, one typically assumes that the locally parallel basic flow changes only slowly in the streamwise x direction and that the WKB formalism is applicable. At each streamwise x station, the instability characteristics are, therefore, to leading-order, given by parallel flow theory. One can then easily envision physical situations in which a convection velocity, say the U parameter introduced in the models of section 3, changes slowly with x . If, at a particular station x_t , U reaches the critical value U_c where the branch point ω_0 crosses the real ω -axis, the flow will change from being locally convectively unstable to locally absolutely unstable, or vice-versa. If, more generally, several crossings take place as x is varied, the flow can be divided into several regions where the local absolute growth rate $\omega_{0i}(x)$ is positive or negative. In the border regions where $\omega_{0i}(x_t)$ vanishes, the slowly-varying analysis breaks down, and transition layers of Airy type have to be introduced, as in classical WKB theory.

The particular case of an absolutely unstable domain separating two convectively unstable regions (hereafter referred to as CU-AU-CU) was studied by Pierrehumbert [10] for a zonally-varying two-layer model of the baroclinic instability. Earlier analytical work by Thacker [18] and Merkin [36] had established that the same two-layer model in the parallel approximation underwent a transition from absolute to convective instability above a critical value of the ratio between the average speed of the mean flow and the shear. Pierrehumbert [10]

demonstrated, by a combination of analytical and numerical means, that the slowly-varying baroclinic flow could support modes locally confined along the stream and growing at the *maximum absolute growth rate* $\omega_{0i \max}$ over the entire domain $-\infty < x < \infty$. Thus Pierrehumbert's work suggests a *frequency selection criterion*, whereby, in a mixed flow situation of the type CU-AU-CU, *the dominant frequency is equal to* $\omega_{0r \max}$, *namely the real part associated with the maximum absolute growth rate* $\omega_{0i \max}$ *over the entire flow.*

But, in a study of two-dimensional wakes behind bluff bodies, Koch [35] proposes yet another frequency selection mechanism. According to his analysis, the developing wake is a mixed flow of the type solid body-AU-CU, a characteristic that one might have inferred from the earlier investigation of the $\text{sech}^2 y$ wake by Mattingly & Criminale [3]. *The dominant frequency should, in Koch's scenario, lock to* $\omega_{0r}(x_t) = \omega_0(x_t)$, *i.e., to the real frequency pertaining to the transition point* x_t *separating the AU and CU regions.* Needless to say, $\omega_0(x_t)$ and $\omega_{0r \max}$ are in general distinct and do not lead to the same predictions. A comparison between stability calculations and wake experiments reveals nonetheless that Koch's criterion predicts the shedding frequency of the Karman vortex street relatively well. This appears to imply that intense self-sustained oscillations occur in the AU region between the body and the transition point x_t . This *hydrodynamic resonance phenomenon* is somewhat akin to the resonances which are produced when a shear layer issuing from a streamlined or blunt body interacts with a second body placed at a finite distance downstream [37]. Note, however, that hydrodynamic resonances do not rely on the presence of a second body; the necessary streamwise length scale is generated instead by the flow itself in the form of the distance x_t . A recent analysis by Nguyen [38] further confirms Koch's results: for a two-parameter family of wake velocity profiles which closely fits experimentally-measured mean flows, it is found that the varicose mode is in general CU. The sinuous mode, however, leads to a pocket of AU within the near wake and it is responsible for the onset of self-sustained oscillations.

To close this discussion of frequency selection mechanisms in mixed flows, it is worth mentioning the interesting conjecture of Monkewitz & Sohn [5]. In the view of these authors, one should distinguish between two possible configurations and change the frequency selection criterion accordingly. If the flow is of the type solid body-AU-CU, one should follow Koch's proposition $\omega_0(x_t)$. If it is of the type solid body-CU-AU-CU, one should adopt Pierrehumbert's selection principle $\omega_{0r \max}$. Wakes with initially thick shear layers fall within the first category [38] whereas initially very thin shear layers lead to a wake of the second category. Predictions of shedding frequency for these two families of wakes appear to follow experimental trends provided one adopts Monkewitz & Sohn's recommendation regarding the choice of selection criterion.

The reader is further referred to Monkewitz & Sohn [5] for an interesting application of absolute and convective instability concepts to the control of hot jets. Viscous liquid jets have also been examined in this light by Leib & Goldstein [39].

4.4. Absolute instabilities, convective instabilities and chaos

As emphasized by Deissler [40,41] and Deissler & Kaneko [42], the distinction between absolute and convective instabilities plays a crucial role in the search for chaos in transitional flows. Absolutely unstable flows such as Rayleigh-Bénard convection or Taylor-Couette flow can give rise, under carefully controlled conditions, to chaotic motion on a low dimensional attractor (see, for instance, Bercé, Pomeau, Vidal [43]). The motion in phase space can usually be reconstructed from a time series at a single point in physical space. Quantitative statistical measures of disorder such as the Lyapunov exponents, fractal dimension and Kolmogoroff entropy can be calculated for each attractor, independently of initial conditions within each basin of attraction. As one would expect in an absolutely unstable flow, low levels of external noise do not alter significantly statistically-averaged quantities on the attractor. In other words, chaos in absolutely unstable flows is *intrinsically* driven by temporally-developing instabilities at each spatial location. As a result, search for chaos in absolutely unstable flows has been reasonably successful, both experimentally and numerically.

Such is not the case in convectively unstable media, i.e., boundary layers, shear layers, jets, pipe flow, etc... Here, disturbances at a fixed spatial location eventually die out so that Lyapunov exponents in the laboratory frame are always negative [42]. There is, of course, plenty of experimental evidence to support that turbulence does occur in these flows sufficiently far downstream but one has not been successful in relating it to chaos produced by a deterministic mechanism (except for the Navier-Stokes equations!).

To explore possible alternative strategies, Deissler [40,41] has conducted numerical studies of the Ginzburg-Landau equation, namely,

$$\frac{\partial A}{\partial t} + U \frac{\partial A}{\partial x} - \mu A - (1 + ic_d) \frac{\partial^2 A}{\partial x^2} + (1 + ic_n) |A|^2 A = 0. \quad (75)$$

In its linearized version around $A = 0$, (75) is identical to (23), the model studied in section 3.1. The real coefficient C_n takes distinct values for different flows, as does C_d . When $U = 0$, the basic state $A = 0$ is absolutely unstable and numerical simulations indicate that, for certain values of the parameters C_d and C_n , the trajectories are confined to a low-dimensional chaotic attractor [44,45,46].

Recall from section 3.1. that the motion is convectively unstable when $U > 2[\mu(1 + C_d^2)]^{1/2}$. In this case, a single-frequency forcing applied at $x = 0$ gives rise to a spatially-developing wave in the region $x > 0$. As shown by Deissler, the characteristics of the spatial wave are well predicted by the linear model (see Figures 5a,b) sufficiently close to the source. Further downstream, the wavetrain reaches a finite-amplitude saturated state described by monochromatic nonlinear solutions of (75) at the forcing frequency. More importantly, when the single frequency excitation is replaced by broadband random fluctuations, the external noise is *selectively* amplified by the system

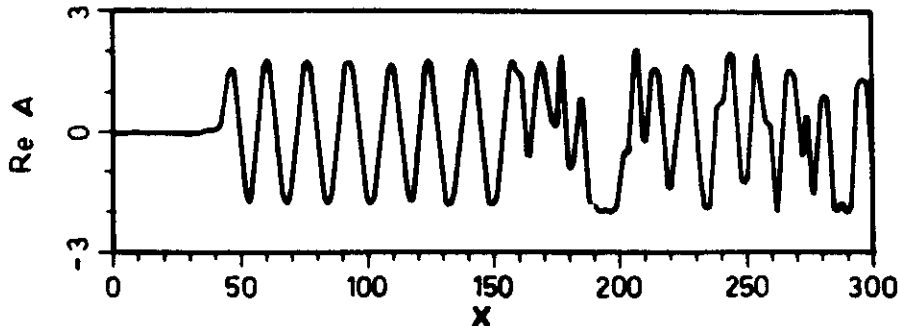


Figure 18. Plot of $\text{Re}A(x,t)$ as a function of x for a given t . The function $A(x,t)$ satisfies the Ginzburg-Landau equation (75). A microscopic noise is added at $x=0$. Reproduced from Deissler [41].

and spatially growing waves are generated at the frequency with the maximum growth rate (see Figure 18). In other words, the initially broad spectrum at $x=0$ shrinks to a narrow spectrum around the most amplified frequency, in the linear region immediately downstream of the source. Further downstream, however, in the finite-amplitude region, the nonlinear wavetrain becomes modulationally unstable to sidebands within the narrow spectrum [47]. This secondary instability brings about a break-up of the primary wave which gradually results in the generation of a broad band spectrum far downstream. As emphasized by Deissler, irregularities in the spatial wave produce random changes in the location of the break-up points, this mechanism being responsible for *intermittency*.

Again, it should be stressed that the fully-developed "turbulent flow" far downstream (Figure 18) is triggered by the external noise fed into the system at $x=0$. In the absence of external fluctuations, no spatial structures can be detected, hence the name *noise-sustained structures* proposed by Deissler. This is in sharp contrast with intrinsic chaos present in absolutely unstable flows, which does not rely for its existence on the presence of external noise.

It remains to answer the following question: If "turbulent flow" in the convectively unstable Ginzburg-Landau equation is induced by external noise, can it legitimately be regarded as deterministic *intrinsic* chaos? In other words, do the usual statistical measures of chaos (dimension, Lyapunov exponents, ...) far downstream become independent of the external noise applied at $x=0$? Until now, no satisfactory answer appears to have been given to this question.

But there are other problems. As noted by Deissler & Kaneko [42], the usual definition of Lyapunov exponents at a *fixed* spatial location always gives a negative number, a fact presumably related to the negative absolute growth rates prevailing in convectively unstable

flows. To arrive at a meaningful measure of chaos in such flows, one must introduce a velocity-dependent largest Lyapunov exponent $\lambda(v)$, obtained by extending the usual definition to a region $\{x_1 + vt, x_2 + vt\}$ in a frame of reference moving at the velocity v . Deissler & Kaneko [42] then propose to call a convectively unstable flow chaotic if the maximum value λ_m of $\lambda(v)$ over all values of v converges to a positive value. In the case of the Ginzburg-Landau equation, a maximum positive value is obtained when $v = U$. For further technical details, the reader is referred to Deissler & Kaneko's paper. As previously noted, it is not clear in our view that λ_m is independent of external noise. Recent experimental research (see, for instance, [24] for a review of mixing layers) has indicated that some convectively unstable flows remain remarkably sensitive to external noise at large downstream distances, even in terms of averaged quantities. Receptivity issues and measures of chaos might have to be examined as a whole if one is to make further progress in the description of disorder in convectively unstable media.

ACKNOWLEDGMENTS

The author wishes to thank L. Brevdo, J. M. Chomaz, P. Couillet, R. J. Deissler, P. A. Monkewitz and L. G. Redekopp for helpful discussions and suggestions. This work is supported by the Air Force Office of Scientific Research under AFOSR Contract No. F49620-85-C-0080. Its presentation at the Workshop on Instabilities and Nonequilibrium Structures held in Valparaíso, Chile on December 16-21, 1985, was made possible thanks to an invitation of the Universidad Técnica Federico Santa María, Valparaíso.

REFERENCES

- [1] R. J. Briggs. *Electron-Stream Interaction with Plasmas*, Research Monograph No. 29, M.I.T. Press, Cambridge, Mass., 1964.
- [2] A. Bers. *Linear Waves and Instabilities*, in *Physique des Plasmas*, C. DeWitt & J. Peyraud (Ed.), Gordon & Breach, New York, 1975.
- [3] G. E. Mattingly & W. O. Criminale. *J. Fluid Mech.*, **51**, 233, 1972.
- [4] P. Huerre & P. A. Monkewitz. *J. Fluid Mech.*, **159**, 151, 1985.
- [5] P. A. Monkewitz & K. D. Sohn. *Absolute Instability in Hot Jets and Their Control*, AIAA Paper No. 86-1882, 1986.
- [6] P. Huerre. *J. Méca Théor. Appl.*, Special Issue on Two-Dimensional Turbulence, 121-145, 1983.
- [7] D. W. Bechert. *Excitation of Instability Waves*, Proc. Symposium IUTAM Aero et Hydro-Acoustique, Lyon, 1985.
- [8] N. Bleistein & R.A. Handelsman. *Asymptotic Expansions of Integrals*, Holt, Rinehart & Winston, New York, 1975.
- [9] C. M. Bender & S. A. Orszag. *Advanced Mathematical Methods for Scientists and Engineers*, McGraw-Hill, New York, 1978.
- [10] R. T. Pierrehumbert. *J. Atmos. Sci.*, **41**, 2141, 1984.

- [11] R. T. Pierrehumbert. Spatially Amplifying Modes of the Charney Baroclinic Instability Problem, Preprint, Princeton University, 1985.
- [12] A. C. Newell & J. A. Whitehead. *J. Fluid Mech.*, 38, 279, 1969.
- [13] L. A. Segel. *J. Fluid Mech.*, 38, 203, 1969.
- [14] K. Stewartson & J. T. Stuart. *J. Fluid Mech.*, 48, 529, 1971.
- [15] J. Pedlosky. *J. Atmos. Sci.*, 29, 680, 1972.
- [16] M. A. Weissman. *Phil. Trans. R. Soc. Lond.*, A290, 639, 1979.
- [17] C. G. Lange & A. C. Newell. *SIAM J. Appl. Math.*, 21, 605, 1971.
- [18] W. C. Thacker. *Geophys. Fluid Dyn.*, 7, 271, 1976.
- [19] M. Abramowitz & I. A. Stegun. *Handbook of Mathematical Functions*, National Bureau of Standards, Washington D.C., 1964.
- [20] F. Roddier. *Distributions et Transformation de Fourier*, McGraw-Hill, Paris, 1978.
- [21] A. Michalke. *J. Fluid Mech.*, 23, 521, 1965.
- [22] P. A. Monkewitz & P. Huerre. *Phys. Fluids*, 25, 1137, 1982.
- [23] T. F. Balsa. Three-Dimensional Wavepackets and Instability Waves in Free Shear Layers, University of Arizona preprint, 1985.
- [24] C. M. Ho & P. Huerre. *Ann. Rev. Fluid Mech.*, 16, 365, 1984.
- [25] M. Gaster. *J. Fluid Mech.*, 22, 433, 1965.
- [26] M. Gaster. *Phys. Fluids*, 11, 723, 1968.
- [27] M. Gaster. *Proc. R. Soc. Lond.*, A347, 271, 1975.
- [28] M. Gaster. The propagation of wavepackets in laminar boundary layers: asymptotic theory for non-conservative wave systems, Preprint, National Maritime Institute, Teddington, England, 1980.
- [29] P. G. Drazin & W. H. Reid. *Hydrodynamic Stability*, Cambridge University Press, Cambridge, 1981.
- [30] A. Michalke. *Z. Flugwiss.*, 19, 319, 1971.
- [31] F. H. Busse. in *Topics in Applied Physics*, 45, Springer-Verlag, Berlin, 1981.
- [32] P. Hall. *J. Fluid Mech.*, 130, 41, 1983.
- [33] S. A. Thorpe. *J. Fluid Mech.*, 46, 299, 1971.
- [34] A. Michalke. *J. Fluid Mech.*, 19, 543, 1964.
- [35] W. Koch. *J. Sound and Vib.*, 99, 53, 1985.
- [36] L. O. Merkin. *Geophys. Astrophys. Fluid Dyn.*, 9, 129, 1977.
- [37] D. Rockwell & E. Naudascher. *Ann. Rev. Fluid Mech.*, 11, 67, 1979.
- [38] L. N. Nguyen. Frequency Selection in Jets and Wakes, Master of Science Thesis, U.C.L.A., Los Angeles, California, 1986.
- [39] S. J. Leib & M. E. Goldstein. *Phys. Fluids*, 29, 952, 1986.
- [40] R. J. Deissler. *J. Stat. Phys.*, 40, 371, 1985a.
- [41] R. J. Deissler. Spatially Growing Waves, Intermittency and Convective Chaos in an Open-Flow System, Los Alamos Report LA-UR-85-4211, 1985b.
- [42] R. J. Deissler & K. Kaneko. Velocity-Dependent Liapunov Exponents as a Measure of Chaos for Open Flow Systems, Los Alamos Report LA-UR-85-3249, 1985.
- [43] P. Bergé, Y. Pomeau & C. Vidal. *L'Ordre dans le Chaos*, Herman, Paris, 1984.
- [44] Y. Kuramoto. *Prog. Theor. Phys. Suppl.*, 64, 346, 1978.
- [45] H. T. Moon, P. Huerre & L. G. Redekopp. *Physica D*, 7, 135, 1983.
- [46] L. R. Keefe. *Stud. Appl. Math.*, 73, 91, 1985.

- [47] J. T. Stuart & R. C. DiPrima. *Proc. R. Soc. London*, A362, 27, 1978.

